Thermal efficiency investigation of a ferrofluid-based cylindrical solar collector with a helical pipe receiver under the effect of magnetic field

Ehsan Shojaeizadeh[a, *], Farzad Veysi[a], Hossein Habibi[b], Koorosh Goodarzi[c], Mehrdad Habibi[d]

[a] Mechanical Engineering Department, Razi University, Kermanshah, Iran
[b] School of Computing, Engineering, and Digital Technologies, Teesside University, Tees Valley, Middlesbrough TS1 3BX, UK.
[c] Department of Mechanical Engineering, Yasouj University, Yasouj 75918-74831, Iran
[d] Department of Electrical Engineering, Iran University of Science and Technology (IUST), Tehran, Iran

Abstract

This experimental study investigates the advantage of using Mn–Zn Fe_2O_4/water ferrofluid subjected to the effect of a non-uniform magnetic field on the thermal efficiency of a fabricated cylindrical solar collector with a receiver in the shape of the helical pipe. Using ASHRAE Standard, this study has investigated the influence of the nanoparticles volume fraction (0.0–1.0%), the mass flow rate of fluid (0.00415-0.033 kg/s), and the produced non-uniform magnetic field by a set of permanent magnets (B_r = 0.0–1.2 T) on the collector' thermal efficiency. The results show that for the ferrofluid, the overall thermal efficiency of the collector is increased with the volume fraction augmentation. For the case with the flow rate of 0.033 kg/s and the volume fraction of 1.0%, the maximum collector efficiency enhancement compared with water has been 48.54%. The positive effect of applying the magnetic field predominates at lower flow rates and higher volume fractions. In the case with the flow rate of 0.00415 kg/s and the volume fraction of 1.0%, by applying the magnets with B_r = 1.2 T, the collector's maximum efficiency is increased by 26.8% compared with that without a magnetic field.

Keywords: Magnetic field; Mn–Zn Fe_2O_4/water ferrofluid; Cylindrical solar collector; Helical pipe; Thermal efficiency; ASHRAE Standard.

*** Corresponding authors. Tel.: +98 831 4274536; fax: +98 831 4283263.**
E-mail address: Ehsan_Shojaeizadeh@yahoo.com (E. Shojaeizadeh).

1. Introduction

Solar collectors absorb solar energy, one of the renewable energies, and transform it as heat to a working fluid (e.g., water and oil) for many domestic and industrial applications. Evacuated tube solar collectors lose lower thermal energy and correspondingly produce higher thermal efficiency than flat-plate ones. Using helical copper pipe to transmit working fluid in a cylindrical evacuated glass can be categorized as one of the evacuated tube solar collectors. The advantage of the helical pipes is the presence of a centrifugal force that induces secondary flow in the pipes and correspondingly increases heat transfer of the collectors [**1**].

Adding nanoparticles (ranging from 10 to 100 nm) to the base fluid (i.e., preparing a nanofluid) is a known method in improving the thermal conductivity of the working fluid and correspondingly thermal efficiency-enhancing of the solar collectors. Since the last decade, many studies have been published concerning the use of conventional nanofluids in the solar collectors. About application of nanofluids, as heat transfer media, in the cylindrical solar collector with a receiver in the shape of the helical pipe, Goudarzi et al. [**2**] have studied experimentally thermal efficiency of a fabricated type of this solar collector with the use of CuO-H_2O nanofluid as heat transfer media. For the nanofluid with a flow rate of 0.0083 kg/s, they showed that the maximum thermal efficiency is increased by 25.6% compared to water. Also, Goudarzi et al. [**3**], in an experimental study, investigated the influence of Al_2O_3–H_2O and CuO–H_2O nanofluids with various pH values on the efficiency of the helical cylindrical solar collector. They showed that the more acidic or basic nanofluid, the more the collector efficiency. Also, for nanofluids with pH values far from the isoelectric point, the collector efficiency is more augmented with Al_2O_3 nanofluid than that with CuO nanofluid. Furthermore, Noghrehabadi et al. [**4**] experimentally showed an enhancement in the thermal efficiency of a conical solar collector with a receiver in the shape of a conical helical pipe containing SiO_2 nanofluid compared with water as working fluid. The Authors in these three studies [**2-4**] have mentioned that the primary mechanism of enhancing the collectors' thermal efficiency is the thermal conductivity augmentation of the base fluids due to the nanoparticles' presence.

As another option that can help enhance heat transfer of large-scale devices like solar collectors is using a magnetic nanofluid (or namely ferrofluid; a composition of a non-conducting base fluid (i.e., water) and dispersed single-domain magnetic nanoparticles) as

working fluid subject to a magnetic field [**5**]. Gan Jia Gui et al. [**6**] by investigating a ferrofluid in a microchannel under the influence of the magnet and Liu et al. [**7**] by studying a ferrofluid in a parabolic trough solar collector subjected to the effect of the electromagnet have mentioned that forming chain-like bridges of the magnetic nanoparticles can enhance the thermal conductivity of the ferrofluids. Also, by subjecting a ferrofluid to a magnetic field, an additional body force (i.e., Kelvin body force: $\mu_0 M \nabla H$ [**8**]) is added to the momentum equation, and correspondingly, its flow scheme and heat transfer can be directed. Ferrofluids' main attribute is their ability to interact with an applied magnetic field. This process of using Kelvin force in controlling heat and fluid flow is called ferrohydrodynamics (FHD) [**8**].

Recently, several types of investigations have been performed about using magnetic nanoparticles in solar thermal collectors. Xu et al. [**9**], in an experimental study, investigated an evacuated tube solar collector having a coated tube by magnetic nanoparticles (i.e., Fe nanoparticles with 180 nm average diameter) to increase the captured solar light and correspondingly enhance the thermal efficiency of the collector. They showed that this technique had improved the captured solar light. Also, the maximum thermal efficiency of the proposed collector has been augmented by 80% compared to that of an ordinary one. Liu et al. [**7**] investigated Fe_3O_4/water ferrofluid as the heat transfer media in a laboratory parabolic trough solar collector influenced by the effect of a magnetic field generated by three separate electromagnets (with produced magnetic field parallel to the fluid flow). They indicated that ferrofluids have higher thermal efficiency values than that of the base fluid, namely water. Also, by applying a magnetic field with a strength of 10.47 mT, the collector's thermal efficiency (with 0.02 kg/s mass flow rate of the fluid) has increased up to 41%. Ameri and Eshaghi [**10**], in a numerical investigation, studied a novel flat-plate solar collector equipped with tubes inserted porous media and Fe_3O_4/water ferrofluid as its heat transfer media subjected to the effect of the magnetic field generated by several electromagnets. According to their results, for Reynolds number of about 736 and the magnetic field strength of 400 G, Nusselt number of the collector with 2.0% weight fraction of the nanoparticles is augmented 1.36 times compared with a similar conventional collector. Also, for this condition, by applying the magnetic field, the collector's thermal efficiency has increased about 0.5% in comparison with a same in shape traditional solar collector. Sami [**11**], in a numerical study, investigated the effect of a magnetic field produced by an element at the inlet of a magnetic fluid-based flat-plate solar collector on the collector's thermal

efficiency. Based on the positive influence of the magnetic field on the ferrofluids' thermal conductivity enhancement, He concluded that the thermal efficiency of the collector is improved by applying the magnetic field. Balakin et al. [**12**], using a multiphase CFD study, have investigated the thermal efficiency of a direct absorption solar collector with a ferrofluid as heat transfer media subjected to the effect of a magnetic field. According to the results of this study, at an optimum value of the gradient of the magnetic field, the collector's thermal efficiency increases by 30%. Khosravi et al. [**13**] numerically investigated using a Fe_3O_4/Therminol 66 ferrofluid with various volume fractions in a parabolic trough solar collector subjected to the effect of a non-uniform magnetic field. They used a wire bellow and paralleled to the collector tube to produce a transverse magnetic field with the strength in the range between 0 to 500 G. They showed that, for the case study with a volume fraction of 4.0%, by applying the magnetic field and augmenting its strength, the collector's thermal efficiency is increased by 2.3% compared to the one without a magnetic field. Malekan et al. [**14**] performed a similar numerical study to Khosravi et al. [**13**] on the parabolic trough solar collector, but with the difference that the collector tube is equipped with internal fins and two different ferrofluids are considered (i.e., CuO/Therminol 66 and Fe_3O_4/Therminol 66). They indicated that by applying the magnetic field, Fe_3O_4/Therminol 66 had shown a higher impact on enhancing the collector efficiency compared with CuO/Therminol 66. Using ferrofluids in a single-ended evacuated tube solar collectors investigated by Shojaeizadeh et al. [**15**]. They have experimentally studied the effect of Mn–Zn Fe_2O_4/water as heat transfer media on the thermal efficiency of a fabricated single-ended tube solar collector in the laboratory. Their experimental setup was manipulated to be influenced by a non-uniform magnetic field produced by a permanent magnet set. They indicated that when the magnets' strength is 1.0 T, the case studies with the input heat flux of 350 W/m^2 and the nanoparticles volume fraction of 0.5%, the maximum average Nusselt number and thermal efficiency enhancements of the collector have been respectively 73.0% and 47.0%. Bezaatpour et al. [**16**] investigated numerically a ferrofluid-based parabolic solar collector equipped with a rotary tube subjected to the effect of the magnetic field. According to their results, the simultaneous effects of the tube's rotation and the presence of the magnetic field can increase heat transfer inside the absorber tube and correspondingly improve the collector's energy and exergy efficiencies. The maximum enhancements of the energy efficiency (=101%) and exergy efficiency (=24%) compared to the case without applying the magnetic field and the rotational tube has been obtained when the field strength and the tube speed have been respectively 1000 G and 0.4 rad/s.

Ferrofluids prepared with Mn–Zn Fe_2O_4 magnetic nanoparticles have been proposed as a suitable option for FHD investigations due to their higher values of magnetic saturation and permeability, lower value Curie temperature, and more significant thermal conductivity in comparison with those of other magnetic nanomaterials [**17-18**]. This ferrofluid is also temperature-sensitive, which means that its magnetization depends heavily on the temperature variation that causes it to have a relatively high-value pyromagnetic coefficient. It should be noted that the pyromagnetic coefficient is a compelling parameter in augmenting Kelvin's body force [**8**]. As it was seen from the literature, there is no investigation on the effect of the ferrofluids on the thermal efficiency of the cylindrical solar collectors equipped with a helical tube receiver. Also, this type of collector can be fitted with permanent magnets inside its helical tube with the advantage of having a slight effect on the interruption of the input solar radiation. Therefore, the present study aims to investigate experimentally the privilege of Mn–Zn Fe_2O_4/water ferrofluid usage as the working fluid of a fabricated cylindrical solar collector with a receiver in the shape of the helical pipe under the influence of the non-uniform magnetic field produced by a set of permanent magnets on the thermal efficiency enhancement of the collector. After preparing the testing setup and stabilizing Mn–Zn Fe_2O_4/water ferrofluids, the effect of various parameters, like nanoparticles volume fraction (0.0–1.0%), mass flow rate of the fluid (0.00415-0.033 kg/s), and strength of the permanent magnets (B_r = 0.0–1.2 T) on the solar collector's thermal efficiency are to be investigated based on the presented testing method in ASHRAE Standard.

2. Experimental procedure

2.1. Mn–Zn Ferrite ferrofluid preparation

Mn–Zn Ferrites magnetic nanoparticles have been synthesized based on wet chemical co-precipitation technique. $MnCl_2{\cdot}4H_2O$, $FeCl_3{\cdot}6H_2O$, $ZnCl_2$, and NaOH materials with an analytical grade purchased from Merck Industrial and Lab Chemicals Company. $MnCl_2$, $FeCl_3$, and $ZnSO_4$ with respective stoichiometry were dissolved in an appropriate amount of distilled water. After adjusting its pH value using HCL, it was fixed at the temperature of 80 C. Next, the obtained aqueous solution mixed with a boiled solution of NaOH (consists of 500 ml of distilled water and 0.5M NaOH) up to 10 s and stirred utilizing a mechanical agitation for one hour. Briefly, it can be said that the synthesis process of the nanoparticles has been done during the following steps: (a) instant converting metal ions to hydroxide ions; (b) converting hydroxide ions to Mn–Zn Fe_2O_4 nanoparticles at the controlled temperature of

the sample of 100 C for 1hr duration. Finally, the synthesized nanoparticles have been washed using purified water and acetone rinse and next dried at the temperature of 90 C. **Fig. 1 (a)** presents the SEM of the prepared Ferrite particles. The mean diameter of the nanomaterials has been about 46 nm. From the VSM **(Fig. 1 (b)**), which is measured at room temperature, it can result that the coactivity and remanent magnetization of the magnetic nanoparticles are near zero. Therefore, they can be ignored, and correspondingly, the magnetic nanoparticles are superparamagnetic. Also, according to this figure, the saturation magnetization of the nanoparticles is about 46 emu/g. Mn–Zn Fe_2O_4-double distilled water ferrofluids at three different volume fractions of 0.2%, 0.5%, and 1.0%, using C-TAB as a dispersant, have been prepared based on the two-step method (using UP-400S ultrasonic model). Variation of Zeta potential of the samples (using Nano Zetasizer, Malvern Instruments Ltd., UK) used to investigate the prepared samples' stability. **Fig. 1 (c)** shows how the stability of a prepared sample is changed for 22 weeks. As shown from this figure, the sample's stability is maintained for more than 13 weeks ($\zeta > 30$ mV). It should be noted that the ferrofluid's stability has been maintained after being subjected to the effect of the magnetic field. Note that the nanoparticles volume fractions of the ferrofluids can be estimated as follows,

$$\varphi = (m_{np}/\rho_{np})/[(m_{np}/\rho_{np}) + (m_f/\rho_f)] \quad (1)$$

where m_f and m_{np} are the mass of water and the mass of the nanoparticles, ρ_{np} is the density of the nanoparticles, and ρ_f is the water density.

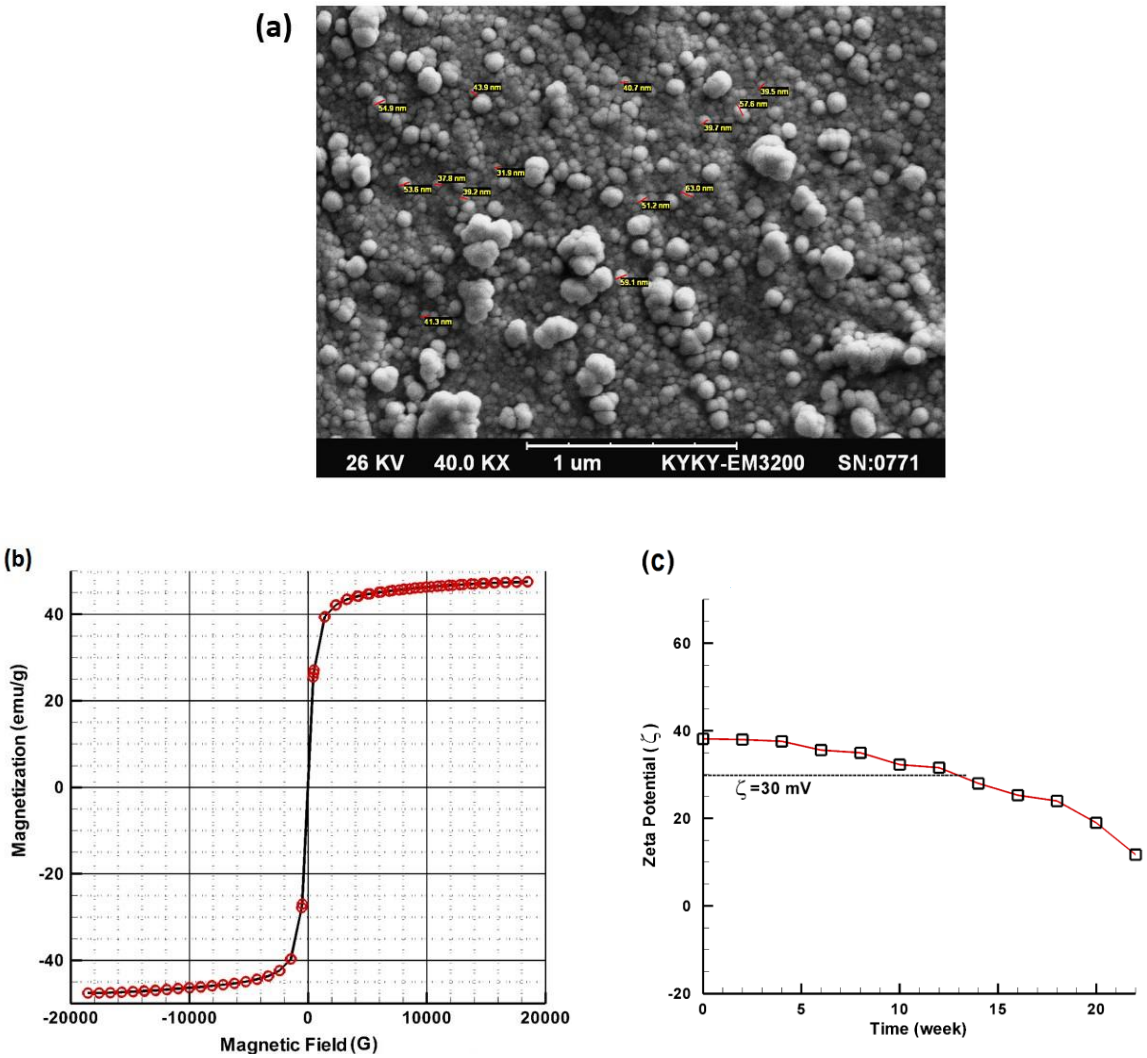

Fig. 1 (a) XRD of Mn–Zn Ferrite nanomaterial, (b) Hysteresis loop of the prepared nanoparticles, and (c) Zeta potential at various times.

2.2 Experimental setup

The basic specifications of the helical tube solar collector are presented in **Table 1**. The schematic and a photograph of the experimental setup are illustrated in **Fig. 2 (a)** and **Fig. 2 (b)**. The experimental investigation on the solar collector has been done at the University of Yasouj, Yasouj, Iran (Longitude: 51° 35' 16.66" E; Latitude: 30° 40' 5.66" N). The main component of the setup is the cylindrical solar collector with helical pipe receiver (1 in **Fig. 2 (a)**) subjecting to the non-uniform magnetic field of four fixed rows of permanent block-magnets (2 in **Fig. 2 (a)**; the four rows display as quadrupole field) inside which. Each row consists of five Neodymium block magnets in line with each other. At each study, the field's strength is changed by substituting the magnets with different remanent magnetizations (B_r = 0.02- 1.2 T). The helical pipe, with spiral rings, painted black and located along with the magnets (note that the magnets of each row were fixed on a Teflon base) inside a well-sealed

cylindrical glass tube (3 in **Fig. 2 (a)**) with minimum reflectivity. Then, the air inside the glass is vacuumed with a vacuum pump. **Fig. 2 (c)** shows the applied magnetic field vectors at an axial cross-section of the helical pipe. It is worth mentioning that when the cases without a magnetic field are supposed to be studied, for having similar physics with the issues subjected to the effect of the magnetic field, the magnets are replaced with the same in size steel blocks. The working fluid of the collector is in a force convection cycle, and it is boosted with a pump (5 in **Fig. 2 (a)**). The flow rate fluid is controlled with the use of a line valve (7 in **Fig. 2 (a)**) and a flow meter (8 in **Fig. 2 (a)**, with the accuracy of 0.01 L/h). It is worth noting that the volume flow meter was calibrated for measuring the mass flow rate of the working fluid (ranging from 0.00415 to 0.033 kg/s) based on the fluid density. Also, for feeding the collector cycle, we used a supplying container (4 in **Fig. 2 (a)**), and for draining it, a drain valve was used (6 in **Fig. 2 (a)**). Furthermore, for transmitting the absorbed thermal load by the collector to water, a heat exchanger (10 in **Fig. 2 (a)**) has been used in an open-loop tank with 20 liters capacity (i.e., a constant water bath temperature) (9 in **Fig. 2 (a)**).

According to **Fig. 2 (a)**, we used three calibrated thermocouples (K type with the accuracy of ±0.1 C) to sense the collector's inlet temperature, the collector's outlet temperature, and the air temperature. A data logger (TES 1384 type; 16 in **Fig. 2 (a)**) was used to read and save the sensor's data. During this study, the solar radiation and wind speed were scrolled respectively by a solar meter (Kipp–Zonen type; with lower than ±2% uncertainty) and an Anemometer (PROVA (AV M-07) type with ±2% uncertainty).

Table 1 General specifications of the setup.

Specification	Dimension/ Value	Unit
Cylindrical copper coil	Length=45, Diameter=12, Coil pitch=1.15	cm
Copper tube	Diameter=0.9525, t=0.063	cm
Evacuated cylindrical glass	Length=48, Diameter=20, t=0.5	cm
Thermal conductivity of the cylindrical glass	k_{Glass}=1.3	W/(m.K)
Thermal conductivity of Cooper	k_{Cu}≈400	W/(m.K)
The glass transmission coefficient	τ=0.76	-
The transmission coefficient of the absorber	α=0.77	-
Permanent magnets at each row (Neodymium Block	10×3×1 (4 in number) & 5×3×1 (1 in number)	cm^3

Magnets)		
Teflon base	45×3.2×1.2	cm^3

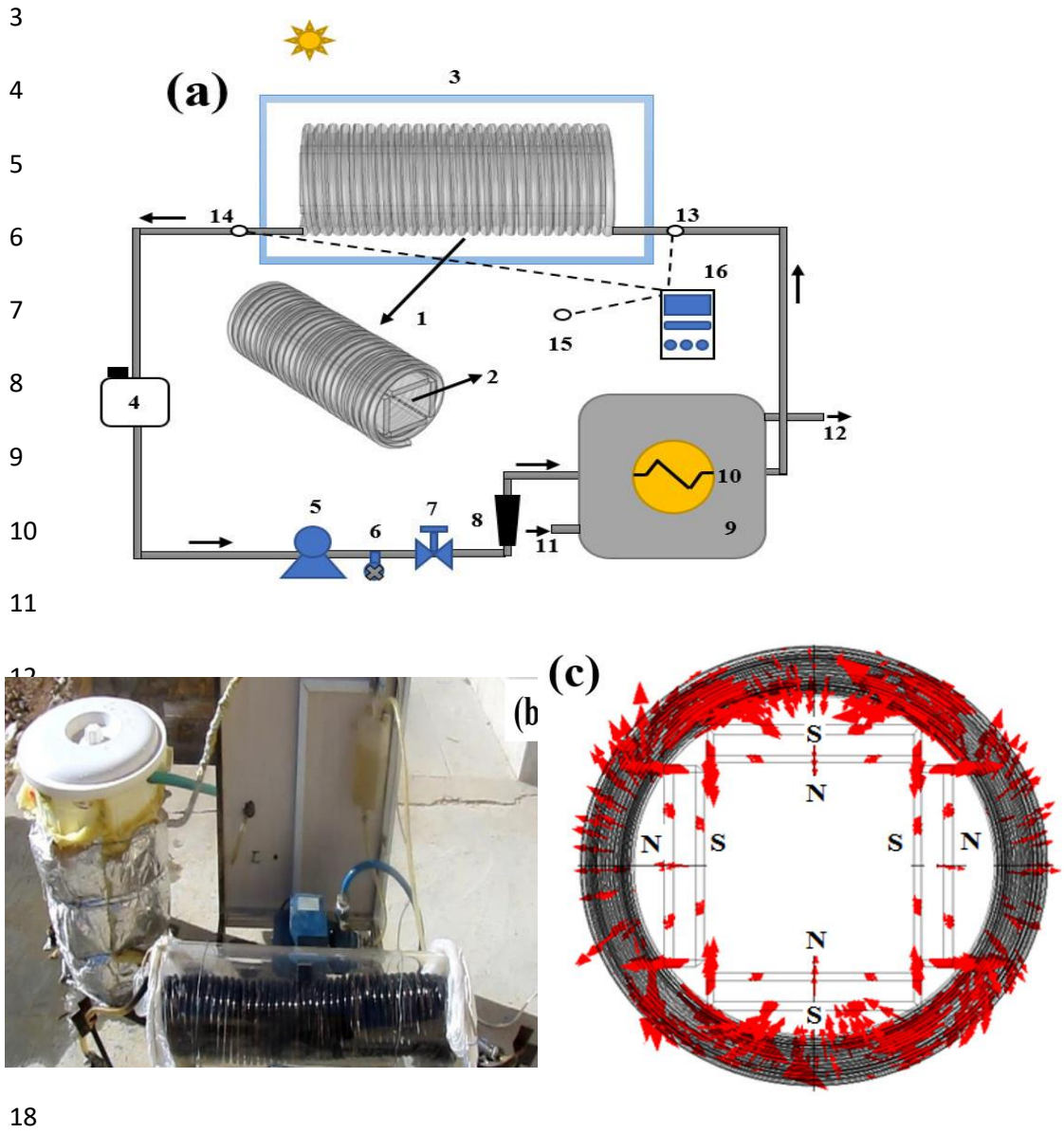

Fig. 2 (a) Schematic of the experimental setup: (1) helical Cu tube, (2) arrangement of the permanent magnets (quadrupole), (3) cylindrical glass, (4) working fluid supply, (5) pump, (6) drain, (7) line valve, (8) flowmeter, (9) tank, (10) heat exchanger, (11) cold water inlet, (12) hot water inlet, (13) collector inlet thermocouple, (14) collector outlet thermocouple, (15) air temperature thermocouple, and (16) thermometer; (b) a photograph of the experimental setup; and (c) distribution of the vectors of the magnetic field produced by the magnets at an axial cross-section.

2.3 Testing method and data reduction

By estimating the ferrofluid as a single-phase fluid and having no internal energy storage, the collector thermal efficiency has been determined using ASHRAE Standard 86–93 [**19**]. According to the mass flow rate of the fluid and the variation of the fluid's temperature in the collector, the received useful energy to the working fluid can be obtained by Eq. (2). Also, according to Eq. (3), the useful energy can be explained in terms of the absorbed energy by the collector and the energy lost from which.

$$Q_u = \dot{m} C_p (T_o - T_i) \quad (2)$$

$$Q_u = A_c F_R \left(G_T (\tau\alpha) - U_L (T_i - T_a) \right) \quad (3)$$

where T_i is the inlet temperature value of the collector, T_o is the outlet temperature value of the collector, C_p is the heat capacity of the working fluid (note that the ferrofluids' heat capacity can be calculated by Eq. (4) [**20**]), $\dot{m}$ is the mass flow rate of the fluid, A_c is the collector's surface area, F_R is the collector's heat removal factor, U_L is the collector's overall heat loss coefficient, and $\tau\alpha$ indicates the product of absorptance–transmittance.

$$\left(\rho C_p\right)_{nf} = \varphi \left(\rho C_p\right)_p + (1 - \varphi) \left(\rho C_p\right)_f \quad (4)$$

In which ρ_{nf}, ρ_f, and ρ_p are respectively the densities of the ferrofluid, water as the base fluid, and the nanoparticles. $\left(C_p\right)_{nf}$ is the ferrofluid's heat capacity, $\left(C_p\right)_p$ is the magnetic nanoparticles' heat capacity, and $\left(C_p\right)_f$ is the water's heat capacity. Not that the working fluid's heat capacity is determined at the mean temperature of the fluid (i.e., $(T_i + T_o)/2$).

Therefore, the instantaneous and overall thermal efficiencies of the collector can be estimated correspondingly by Eq. (5) and (Eq. (6)).

$$\eta_i = Q_u / (A_c G_T) = \left[\dot{m} C_p (T_o - T_i)\right] / (A_c G_T) \quad (5)$$

$$\eta_i = Q_u / (A_c G_T) = F_R (\tau\alpha) - [F_R U_L (T_i - T_a) / G_T] \quad (6)$$

According to ASHRAE Standard, the collector efficiency (η_i from Eq. (6)) can be determined using instantaneous thermal efficiency values (η_i from Eq. (5)), solar radiation near the solar noon (G_T) (i.e., from 10:00 a.m. to 2:00 p.m.), the collector's inlet temperature (T_i) and temperature of the ambient (T_a). In other words, by plotting η_i versus $(T_i - T_a)/G_T$. However, all mentioned parameters, as well as the fluid flow rate ($\dot{m}$), must be maintained at steady-state condition ($\dot{m}$, T_i, T_a, and G_T must not have the variation of more than respectively ±1%, ±0.1 K, ±1.5 K, and ±0.50 W/m^2) during a test period [**19**]. A test period is of a data

period (i.e., the maximum value of the collector time constant and 5 min) and a pre-data period (15 min). Noteworthy is to mention that the collector's time constant (i.e., the needed time for passing the working fluid through the collector to reach 63% of its steady condition value when an immediate change in the radiation is imposed) can be evaluated and used as [**19**],

$$[(T_{o\tau} - T_i)/(T_{oi} - T_i)] = 0.368 \quad (7)$$

where T_i, as mentioned before, is the inlet temperature of the collector, T_{oi} is the initial inlet temperature value of the collector (i.e., before shading on the collector surface), and $T_{o\tau}$ is the outlet temperature of the collector after the time it takes for it to reach a steady-state after shadowing on the surface of the collector. In this study, the time constant of the collector has been less than five min (i.e., < 5 min) in all tested mass flow rates (0.0415-0.033 kg/s).

By performing the tests near the solar noon, these parameters are almost constant. $F_R(\tau\alpha)$ value (i.e., the maximum thermal efficiency of a solar collector) can be obtained by intersecting the linear trend line of the thermal efficiencies (Eq. (5)) from the averaged value of data period versus $(T_i - T_a)/G_T$ to the vertical axis (i.e., η_i axis). Also, the trend line slope depicts the $F_R U_L$ value. Furthermore, by intersecting the obtained line with the horizontal axis (i.e., $(T_i - T_a)/G_T$ axis), the stagnant point of the collector is obtained. At this point, the collector efficiency is zero.

2.4 Uncertainty analysis

The uncertainty with the confidence level of 95% linked to the calculations has been done using the single sample uncertainty model (Eq. (8)) [**21**]. The absolute and relative uncertainties connected to the thermal efficiency (Eq. (5)), as a function of different independent variables ($\dot{m}$, $\Delta T_{oi} = (T_o - T_i)$, and G_T) (not that errors connected to A_c and C_p were neglected) calculated at least three times, relatively based on the following single sample model,

$$\delta\eta_i = \left[\left((\partial\eta_i/\delta\dot{m})\delta\dot{m}\right)^2 + ((\partial\eta_i/\delta\Delta T_{oi})\delta\Delta T_{oi})^2 + \left((\partial\eta_i/\delta G_T)\delta G_T\right)^2\right]^{1/2} \quad (8a)$$

$$\delta\eta_i = [(\partial\dot{m}/\dot{m})^2 + (\partial\Delta T_{oi}/\Delta T_{oi})^2 + (\partial G_T/G_T)^2]^{1/2} \quad (8b)$$

From the uncertainty calculations, the maximum connected uncertainty of the collector thermal efficiency has been 5.1%.

3. Results and discussion

This experimental study applies ASHRAE Standard and investigates the thermal efficiency of the ferrofluid-based cylindrical solar collector with and without the presence of the magnetic field. To better explore the advantage of the ferrofluid-based solar collector, all the obtained data are compared with water as the traditional working fluid of the collector. This investigation was performed outdoor. So, it was time-consuming to need various days for having the best experimental data with similar weather and solar radiation conditions.

For water with a mass flow rate of 0.00415 kg/s, a testing day with recorded temperature and solar radiation data are presented in **Fig. 3**. As seen from this figure, the tests have been performed around the solar noon (i.e., from 10:00 a.m. to 2:00 p.m.). As described in Section 2.3, the length of this testing time includes four 60 min test runs, and each test run contains three test periods. Also, at each test run, the fluctuations in the collector inlet temperature, ambient temperature, fluid flow rate, and solar radiation have been respectively less than 0.9 C, 0.2 C, 0.09%, and 50 W/m^2.

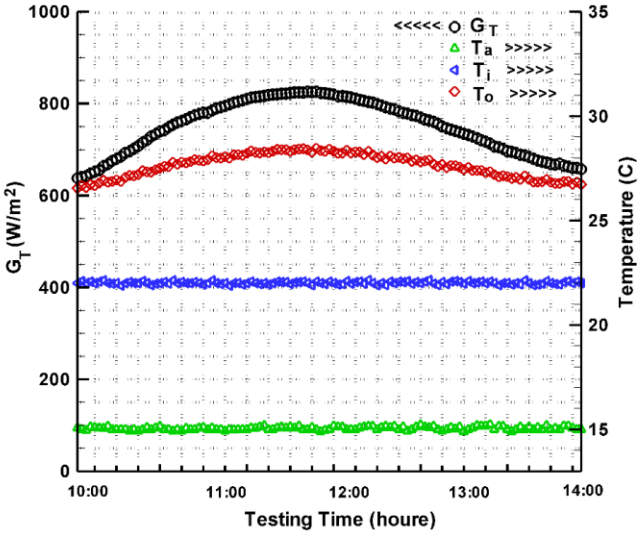

Fig. 3 A testing day for the case with water at 0.00415 kg/s mass flow rate of the fluid.

3.1 Water as the working fluid

At first, the collector's thermal efficiency was investigated with water at different fluid flow rates (i.e., 0.00415, 0.0083, 0.0167, and 0.083 kg/s). For the four flow rates, **Fig. 4** shows the collector efficiency variation against $(T_i - T_a)/G_T$. The linear trend line of the thermal efficiencies (Eq. (5)) is plotted to provide ASHRAE Standard parameters ($F_R(\tau\alpha)$ and

$F_R U_L$). These parameters are presented in **Table 2**. According to the results, $F_R(\tau\alpha)$ is almost unchanged with the flow rate increase. However, the higher the flow rate, the lower the $F_R U_L$ value. For example, with the flow rate augmentation from 0.00415 to 0.033, the $F_R U_L$ value is decreased by 22.5%. Therefore, according to Eq. (6), the overall thermal efficiency is enhanced with fluid flow augmentation.

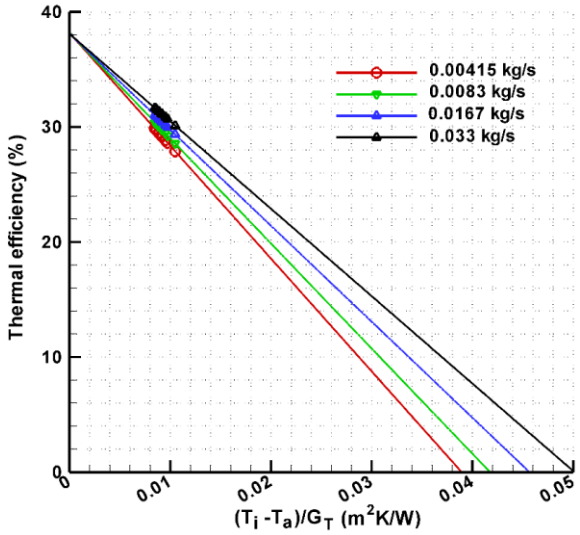

Fig. 4 The collector's thermal efficiency against $(T_i - T_a)/G_T$ for water at different fluid flow rates.

Table 2 Thermal efficiency parameters of the collector for water with various fluid flow rates.

$\dot{m}$ (kg/s)	$F_R(\tau\alpha)$	$F_R U_L$	Time constant (min)
0.00415	0.3817	9.8055	3.1
0.0083	0.3815	9.1395	2.4
0.0167	0.381	8.344	1.6
0.033	0.3809	7.6	0.83

Generally speaking, the fluid inside the helical tube is under the influence of gravity, centrifugal (i.e., secondary flow), and inertial forces. With the fluid passes through the helical tube, a centrifugal force is produced in the fluid flow due to an imposed outward acceleration by the helical curvature to the flow. This centrifugal force can increase heat transfer due to its mixing effect on the fluid media. In other words, the centrifugal force continuously replaces the hot liquid near the wall of the tube with the fluid with lower temperature around the tube center. It means that the thermal boundary layer (δ_t) is decreased near the tube wall. The basic non-dimensional parameter to justify heat transfer behavior in the helical is heat transfer coefficient, as follows,

$$h = (Nu \times k)/D \quad (9a)$$

in which k is the thermal conductivity of the fluid, D is the tube diameter, Nu is fluid's Nusselt number, which can be evaluated as the following correlation [**22**],

$$Nu = \left[\left\{\left[\frac{48}{11} + \frac{51/11}{\left(1+\frac{1342\left[\left(1+(b/2\pi D)^2\right)^{1/2}\right]}{PrDn^2}\right)^2}\right]^3 + 1.816\left[\frac{Dn}{\left(1+\frac{1.15}{Pr}\right)\left[(1+(b/2\pi D)^2)^{1/2}\right]}\right]^{1.5}\right\}\right]^{1/3} \quad (9a)$$

where

$$Dn \sim \frac{\sqrt{\frac{1}{2}(centrifugal\ forces)\times(inertial\ forces)}}{viscous\ forces} = \frac{\sqrt{\left(\rho D^2 D_c \frac{u^2}{D}\right)\times\left(\rho D^2 D_c \frac{u^2}{D_c}\right)}}{\lambda \frac{u}{D} D D_c} = Re \times (D/D_c)^{1/2} \quad (9c)$$

Dn is the Dean number, Pr is the Prandtl number, b is the helical pitch, D_c is the diameter of the helical curvature, and Re is the Reynolds number.

According to Eq. (9), the heat transfer of the collector is directly dependent on the Dn number. It should be noted that with flow rate augmentation, the inertial and centrifugal forces are increased (i.e., Dn is increased), and correspondingly, the velocity and temperature profiles are changed. These changes will lead to the reduction of the wall temperature of the collector tube and a decrease in heat loss from the collector likewise.

3.2 Ferrofluid as the working fluid without applying a magnetic field

To better investigate the collector efficiency, from now on, we primarily focus on the obtained $F_R(\tau\alpha)$ and $F_R U_L$ values and their variations. The obtained $F_R(\tau\alpha)$ and $F_R U_L$ values regarding the three different volume fractions (0.2, 0.5, and 1.0%) at various fluid flow rates are given in **Table 3**. According to the presented data, each value of the specified flow rate range (i.e., $\dot{m}$= 0.00415-0.033 kg/s), $F_R(\tau\alpha)$ is increased with volume fraction augmentation. The maximum $F_R(\tau\alpha)$ increase (i.e., 48.54%) has occurred at the volume fraction of 1.0% with the fluid flow rate of 0.033 kg/s.

Table 3 $F_R(\tau\alpha)$ and $F_R U_L$ values for the ferrofluid at different volume fractions and various fluid flow rates.

φ (%)	$\dot{m}$ (kg/s)	$F_R(\tau\alpha)$	$F_R U_L$
0.2	0.00415	0.4399	10.124
	0.0083	0.4401	9.3675
	0.0167	0.4453	8.5
	0.033	0.4524	7.71

0.5	0.00415	0.4826	10.6
	0.0083	0.4838	9.8
	0.0167	0.4891	9.03
	0.033	0.4915	8.2
1.0	0.00415	0.5336	11.2
	0.0083	0.5462	10.68
	0.0167	0.5513	9.8
	0.033	0.5658	9.15

Fig. 5 depicts $F_R(\tau\alpha)$ and $F_R U_L$ variations for the ferrofluids in different volume fractions and various flow rates compared with those of water. Noteworthy is that the domination of whether $F_R(\tau\alpha)$ or $F_R U_L$ variations values than each other can be a reliable reference in determining the variation of the collector thermal efficiency in different case studies.

According to this figure, for the ferrofluid cases with 0.2, 0.5, and 1.0% volume fractions, the $F_R U_L$ parameter decreased, fluctuated, and increased with increasing fluid flow rate. This figure also shows that in the three mentioned volume fractions, the increase in the $F_R(\tau\alpha)$ value is much higher than that of the $F_R U_L$ value. The higher the volume fraction, the more elevated the collector efficiency enhancement. Compared to water as the heat transfer media, the maximum collector efficiency (i.e., $F_R(\tau\alpha)$) enhancement and the maximum difference between the variations of $F_R(\tau\alpha)$ and $F_R U_L$ values have been respectively 48.54% and 28.15%, which have been occurred for the case with $\dot{m}$= 0.033 kg/s and φ= 1.0%.

As we are all well aware, heat transfer coefficient (i.e., Eq. (9a)) can be approximated by the ratio of k/δ_t, in which k and δ_t are respectively thermal conductivity and thermal boundary layer thickness of the fluid. With increasing nanoparticles volume fraction (φ), the fluid thermal conductivity (k) is increased [**15**]. With the augmentation of the fluid flow rate ($\dot{m}$), the Reynolds number increases, and the thermal boundary layer thickness (δ_t) of the fluid is decreased. Therefore, it can be concluded that the collector heat transfer and correspondingly its thermal efficiency (η_i) is increased with increasing φ and $\dot{m}$ values.

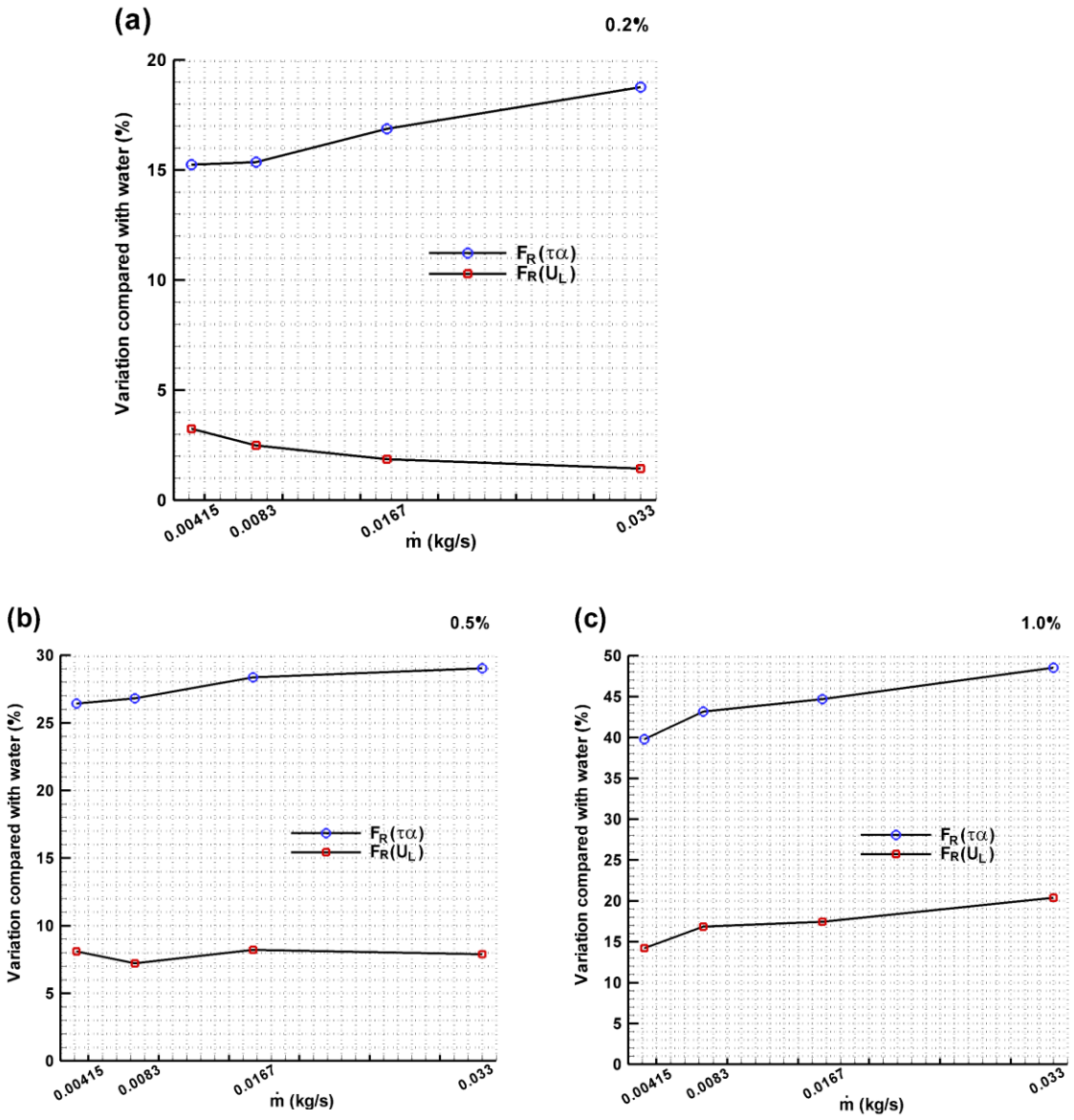

Fig. 5 $F_R(\tau\alpha)$ and $F_R U_L$ variations for the ferrofluid (with (a) 0.2%, (b) 0.5%, and (c) 1.0%) at various flow rates compared with water.

3.3 Ferrofluid as the working fluid subjected to the effect of the magnetic field

In this section, the magnetic field's influence on the efficiency of the ferrofluid-based collector is investigated. At first, for the various case studies (i.e., φ = 0.2, 0.5, and 1.0%; $\dot{m}$= 0.00415-0.033 kg/s; B_r = 0-1.2 T), Section 3.3.1 presents an analysis procedure similar to Section 3.2 for investigating $F_R(\tau\alpha)$ and $F_R U_L$ variations. After that, a comparison between the results of this study and those from the literature is discussed in Section 3.3.2. Lastly, the

role of the magnetic field on the thermal behavior variation of the collector is discussed in Section 3.3.3.

3.3.1 $F_R(\tau\alpha)$ and $F_R U_L$ variations of the Ferrofluid-based collector subjected to the effect of the magnetic field

By imposing the magnetic fields generated by the magnets (B_r= 0.2, 0.5, 0.8, 1.0, and 1.2 T), the experiments have been performed again at different volume fractions as well as various fluid flow rates. $F_R(\tau\alpha)$ and $F_R U_L$ values are presented in **Table 4**. According to this table, it is seen that for all presented cases, the $F_R U_L$ value is decreased with increasing imposed magnetic field. This decrease indicates a beneficial effect on the efficiency enhancement due to the reduction of the heat loss parameter (i.e., $F_R U_L$ in Eq. (6)).

Based on the presented data in **Tables 3-4**, **Fig. 6** represents $F_R(\tau\alpha)$ values for the ferrofluids (0.2%, 0.5%, and 1.0%) at different fluid flow rates ($\dot{m}$= 0.00415-0.033 kg/s) under the effect of different remanent magnetizations (B_r = 0-1.2 T). Also, with the use of the presented data in **Tables 3-5**, **Fig. 7** represents the subtraction between $F_R(\tau\alpha)$ and $F_R U_L$ variations for the ferrofluids with the three different volume fractions at various flow rates under the effect of the different remanent magnetizations compared with water. This figure assumes the same order for $F_R(\tau\alpha)$ and $F_R U_L$ parameters in Eq. (6) and tries to show the beneficial effect of the magnetic field on the collector efficiency using the two mentioned parameters.

From these figures (**Figs. 6-7**), it is seen that the two figures have almost the same trend, which can be concluded that $F_R(\tau\alpha)$ augmentation dominates over $F_R U_L$ increase. Also, from these figures, there is an evident connection between the beneficial effect of the magnetic field on the collector efficiency and the field strength, volume fraction, and fluid flow rate values (refer to discussions in Section 3.3.3). The beneficial effect of the applied magnetic field predominates at lower flow rates and higher volume fractions. This effect is increased with magnetic field augmentation. Therefore, by focusing on the maximum thermal efficiency values (i.e., $F_R(\tau\alpha)$) from **Fig. 6**, the main effect of the magnetic field on the maximum collector efficiency enhancement has been obtained at the lowest mass flow rate value (i.e., $\dot{m}$= 0.00415 kg/s). This effect is reduced with increasing fluid flow rate. The maximum $F_R(\tau\alpha)$ enhancement compared with water is 67.67%, obtained for the case with φ = 1.0%. To put it another way, for the case study with $\dot{m}$= 0.00415 and φ = 1.0%, by

applying the magnets with B_r = 1.2 T the collector's maximum efficiency is increased by 26.8% compared to that of the case without a magnetic field.

Table 4 $F_R(\tau\alpha)$ and $F_R U_L$ values at various volume fractions, fluid flow rates, and remanent magnetizations.

φ =0.2%										
B_r (T)	0.2		0.5		0.8		1.0		1.2	
$\dot{m}$ (kg/s)	$F_R(\tau\alpha)$	$F_R U_L$	$F_R(\tau\alpha)$	$F_R U_L$	$F_R(\tau\alpha)$	$F_R U_L$	$F_R(\tau\alpha)$	$F_R U_L$	$F_R(\tau\alpha)$	$F_R U_L$
0.00415	0.445	10.09	0.449	9.8	0.4518	9.5	0.459	9.3	0.461	8.95
0.0083	0.4408	9.3	0.447	9.25	0.449	9.2	0.453	9	0.4572	8.7
0.0167	0.4451	8.49	0.446	8.5	0.45	8.55	0.454	8.55	0.454	8.4
0.033	0.4525	7.72	0.4525	7.72	0.454	7.73	0.456	7.73	0.456	7.7
φ =0.5%										
B_r (T)	0.2		0.5		0.8		1.0		1.2	
$\dot{m}$ (kg/s)	$F_R(\tau\alpha)$	$F_R U_L$	$F_R(\tau\alpha)$	$F_R U_L$	$F_R(\tau\alpha)$	$F_R U_L$	$F_R(\tau\alpha)$	$F_R U_L$	$F_R(\tau\alpha)$	$F_R U_L$
0.00415	0.495	10.4	0.51	10.25	0.522	10.1	0.531	9.9	0.54	9.5
0.0083	0.49	9.7139	0.501	9.7	0.515	9.65	0.524	9.6	0.53	9.3
0.0167	0.4912	9.03	0.494	8.95	0.5	8.88	0.506	8.8	0.515	8.7
0.033	0.492	8.21	0.492	8.2	0.494	8.2	0.495	8.18	0.499	8.14
φ =1.0%										
B_r (T)	0.2		0.5		0.8		1.0		1.2	
$\dot{m}$ (kg/s)	$F_R(\tau\alpha)$	$F_R U_L$	$F_R(\tau\alpha)$	$F_R U_L$	$F_R(\tau\alpha)$	$F_R U_L$	$F_R(\tau\alpha)$	$F_R U_L$	$F_R(\tau\alpha)$	$F_R U_L$
0.00415	0.553	11	0.576	10.9	0.598	10.7	0.619	10.5	0.64	10.3
0.0083	0.552	10.55	0.566	10.44	0.585	10.3	0.612	10.2	0.6324	10
0.0167	0.551	9.7	0.56	9.6	0.571	9.5	0.588	9.4	0.6	9.3
0.033	0.566	9.1	0.567	8.95	0.567	8.9	0.573	8.8	0.578	8.6

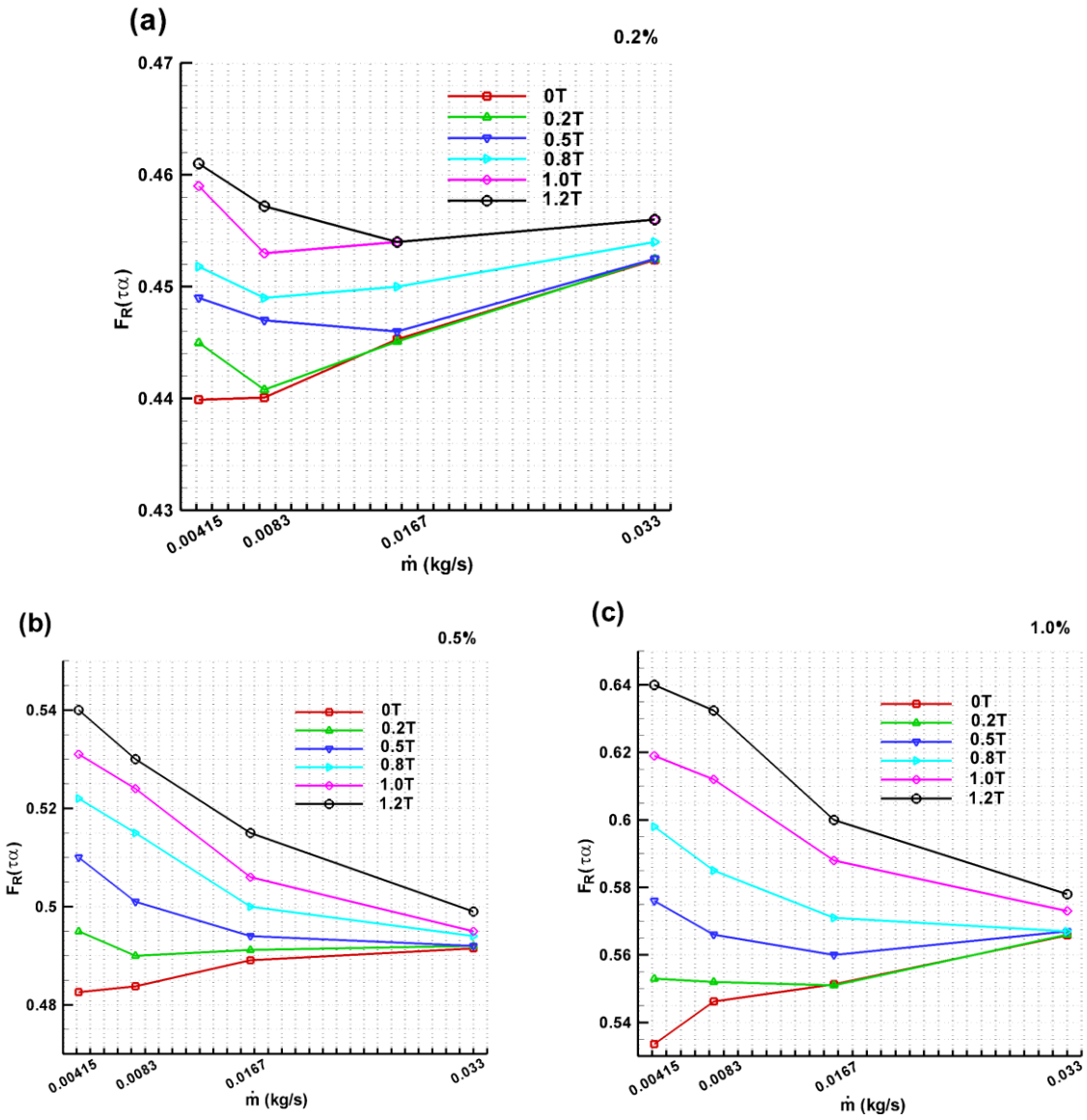

Fig. 6 $F_R(\tau\alpha)$ values for the ferrofluid (with (a) 0.2%, (b) 0.5%, and (c) 1.0%) at various flow rates under the effect of various remanent magnetizations.

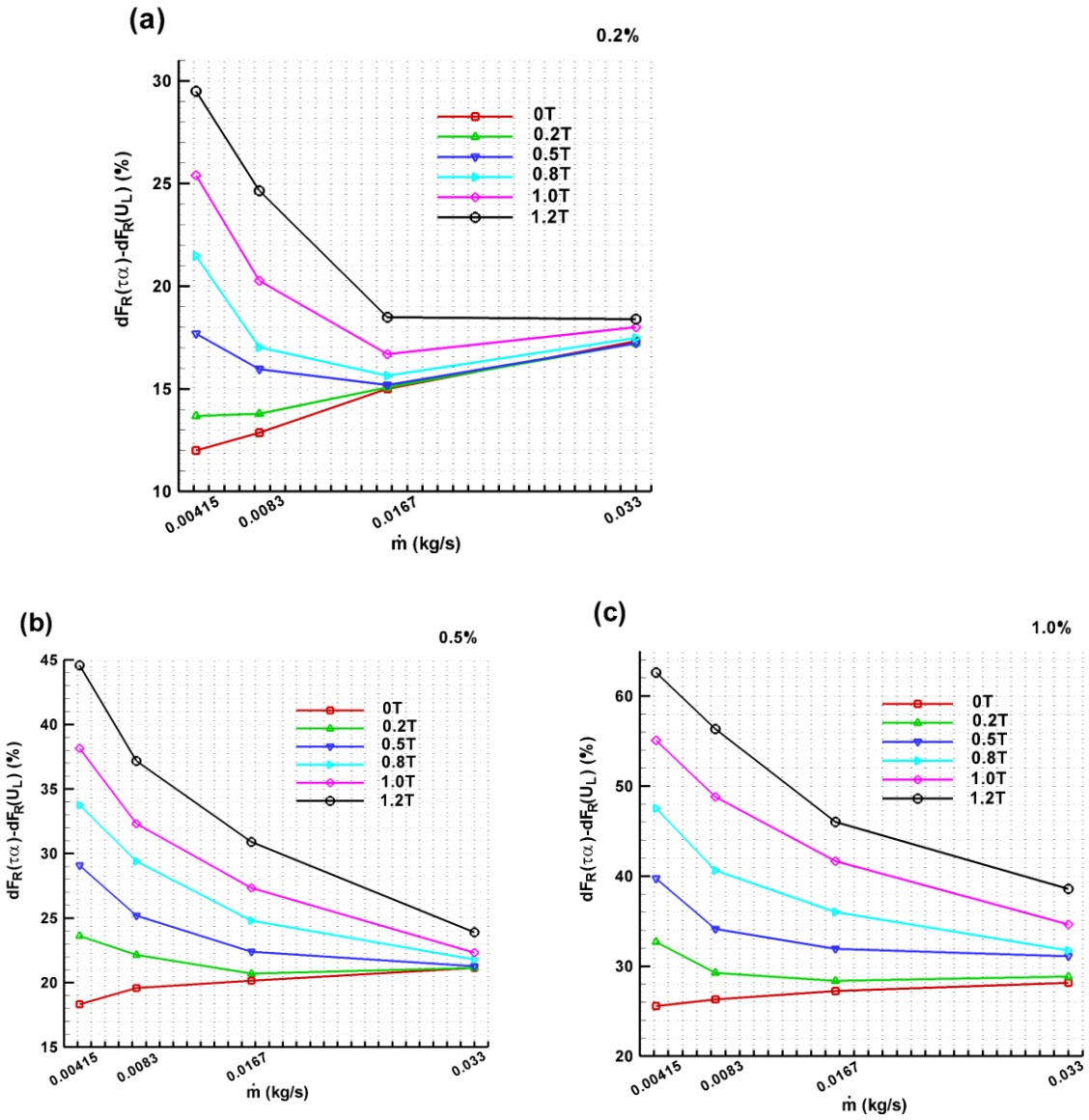

Fig. 7 Subtraction between $F_R(\tau\alpha)$ and $F_R U_L$ variations for the ferrofluid (with (a) 0.2%, (b) 0.5%, and (c) 1.0%) at various flow rates under the effect of various remanent magnetizations compared with water.

3.3.2 A comparison between the results of this study and those from the literature

Table 5 compares the obtained maximum thermal efficiency enhancement compared with water from this study, for the volume fraction case of 0.2%, with $\dot{m}$=0.0083 kg/s and $\dot{m}$=0.033 kg/s, to those of resulted by respectively Goudarzi et al. [**2**] (CuO/water with 40 nm in size nanoparticles) and Goudarzi et al. [**3**] (Al_2O_3/water with 20 nm in size nanoparticles). It should be noted that pH values of the ferrofluid in this study and the studied nanofluids (CuO/water and Al_2O_3/water) by Goudarzi et al. [**2-3**] are at almost the same value. However,

there is a difference in Dean numbers (i.e., De; Eq. (9c)), nearly other weather conditions, and the being vacuum option in the present study.

According to this table, the enhancement of $F_R(\tau\alpha)$ in the present study is lower than those obtained by Goudarzi et al. [**2-3**]. According to Eq. (9), this weakness is because the thermal conductivity of the magnetic nanoparticles (i.e., Mn–Zn Fe_2O_4; k=29 W/(m. K) [**17**]) is lower than those of the two studied nanoparticles (CuO and Al_2O_3). Also, as the helical diameter in this study (D=12 cm) is higher than those helical diameters (D=10 cm), the centrifugal force in their helical tube is more noticeable than that in this study. Correspondingly the heat transfer coefficient (i.e., Eq. (9)) of their collector is higher than the one in this study. Furthermore, the helical length (L= 45 cm) in this study is lower than those helical length (L= 60 cm). This deficiency leads to lower heat transfer [**23**].

However, despite all the mentioned differences, according to this table, the effect of the ferrofluid on the $F_R(\tau\alpha)$ increase is augmented with the field's rise. As aforementioned, the impact of the magnetic field on the collector efficiency augmentation predominates at higher volume fraction values. So, it can be said that the ferrofluid has an adequate ability to compete with other nanofluids.

Table 5 A comparison between $F_R(\tau\alpha)$ increase compared with water in the present study and those obtained by Goudarzi et al. [**2-3**].

$\dot{m}$=0.0083 kg/s			$\dot{m}$=0.033 kg/s		
	B_r (T)	$F_R(\tau\alpha)$ increase (%)		B_r (T)	$F_R(\tau\alpha)$ increase (%)
Al_2O_3/water [**3**]	-	33.16	CuO/water [**2**]	-	20.94
Mn–Zn Fe_2O_4/water	0	18.77	Mn–Zn Fe_2O_4/water	0	15.36
	0.2	18.8		0.2	15.54
	0.5	18.8		0.5	17.17
	0.8	19.19		0.8	17.7
	1	19.7		1	18.74
	1.2	19.7		1.2	19.84

3.3.3 Description of the role of the magnetic field on the collector heat transfer

The permanent magnets in this study generate non-uniform magnetic fields. The magnetic flux density distribution is depicted in **Fig. 8**.

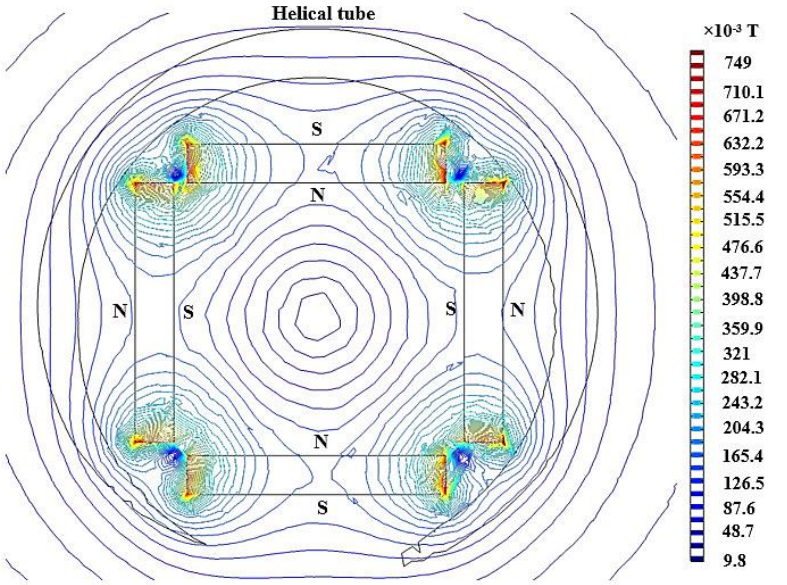

Fig. 8 Distributed magnetic flux density using the set of magnets with B_r= 1.0 T.

This figure indicates that the maximum flux density and correspondingly output energy is consumed between the adjacent opposite poles due to their intense attraction. This inter-pole attraction energy is confronted using tightening the magnets on the Teflon base, and the produced outer field along the magnets is used to affecting the sample domain. The effect of the magnetic field can appear in both laminar and turbulent fluid flows. For example, when a magnetic field is applied to a steady, incompressible, and viscous fluid flow, magnetic body force (F_B) is added to the momentum equation [**15**],

$$\rho(\vec{u}.\nabla)\vec{u} = -\nabla P + \lambda\nabla^2\vec{u} + F_B + f \quad (10)$$

In which λ is the dynamic viscosity of the fluid, F_B is the magnetic force per unit volume as a function of the gradient of the magnetic field, which is called Kelvin body force (Eq. (11) [**8, 24**]), and the last term (i.e., f) indicates another volume forces.

$$F_B = \left[\mu_0(\vec{M}.\nabla)\vec{H} + \frac{\mu_0}{2}\nabla\times(\vec{M}\times\vec{H})\right] \quad (11a)$$

Note that the second term in this equation (Eq. (11a)) is called magnetic dissipation, and M is the magnetization of the ferrofluid, which is defined as follows,

$$M = M_s L(\xi) = \left(6m_p\varphi/(\pi {d_p}^3)\right)\left(coth(\xi) - \frac{1}{\xi}\right) \quad (11b)$$

$$L(\xi) = \mu_0 m_p H/(K_B T) \quad (11c)$$

where M_s is the saturation magnetization of the magnetic nanoparticles, $L(\xi)$ is the Langevin function, m_p is the magnetic moment, φ is the volume fraction of the ferrofluid, d_p is the nanoparticles' mean diameter, μ_0 is the vacuum permeability ($= 4\pi \times 10^{-7}\ \mathrm{H}/m$), H is the intensity of the magnetic field, K_B is the Boltzmann constant ($= 1.38 \times 10^{-23}\ J/K$), and T is the sample's temperature.

It should be noted that another influential term of the presence of the magnetic field is a magnetocaloric effect (i.e., $\mu_0 T(\partial M/\partial T)_H(\partial M/\partial T)$ [**15**]). This term is effective when the magnetic field is varied with time (at a constant temperature), and the magnetic phase of the magnetic nanoparticles is changed (i.e., from superparamagnetic to paramagnetic or vice versa). This magnetocaloric term is added to the energy equation; however, this phenomenon cannot be an effective option to be taken into consideration in this study.

To justify the obtained results of the effect of the non-uniform magnetic field on the collector's thermal efficiency, initially, several justifications based on the literature are presented. After that, the proper justification corresponding to this study is discussed. Ahangar Zonouzi et al. [**25**], by applying a quadrupole magnet around a straight tube, and Goharkhah et al. [**26**], using four electromagnets along a straight tube, have experimentally studied the effect of the non-uniform magnetic field on the heat transfer of the tubes. They have claimed that by applying the magnetic field, a Kelvin body force is exerted to the ferrofluid and attracts it to the tube wall. Correspondingly the thermal boundary layer is decreased, and the fluid mixing due to the radial velocity is increased. Khosravi et al. [**13**] studied numerically the influence of a non-uniform magnetic field (produced by a straight wire below the tube) on the heat transfer of a parabolic trough solar collector. They showed that by applying the magnetic field, the ferrofluid is pulled toward the tube's bottom due to the applied Kelvin body force. Also, two vortices have appeared in the cress section of the tube. About helical tubes under the exposure of a magnetic field, Abadeh et al. [**27**] experimentally investigated a ferrofluid-based helical tube with constant wall temperature subjected to the effect of an applied almost uniform magnetic field at the up and down sections of the helical tube. They have mentioned that in addition to the ferrofluid's pushing toward the tube wall, Thermophoresis and Brownian motions effects have determinative roles in heat transfer enhancement in the ferrofluid-based helical tube. Also, Mohammadpourfard et al. [**28**], in a numerical study, investigated the influence of a non-uniform magnetic field (produced by a straight wire inside an annulus containing fin) on the swirling flow of a ferrofluid. They have mentioned that by applying a non-uniform magnetic field, the

centrifugal force is intensified. Correspondingly, the turbulent behavior of the fluid flow is increased.

In other words, we can say that by applying the magnetic field, a viscous coupling between the nanoparticle motion and water as base fluid produces a radial component of velocity that disorders the flow adjacent to the tube wall. Naturally, to satisfy the continuity condition, an inward motion (corresponding to the pushing force) or motion outward (corresponding to the pulling force) produces.

As mentioned in the experimental Setup section (i.e., Section 2.2), the permanent magnets are so arranged that they behave like a quadrupole field affecting the helical tube from its inside. According to the presented virtual schematic in **Fig. 9 (a)**, the flux density near the inside side of the tube is higher than the other sides, which means that the magnetic field tends to push or pull the ferrofluid toward this side of the tube by its applied Kelvin bod force. This enforced ferrofluid can cause an increase in the fluid velocity and correspondingly lead to the temperature profile change (i.e., a reduction in δ_t and correspondingly an enhancement in the heat transfer coefficient). With paying more attention to the details of the magnetic field effect on the ferrofluid flow, it seems logical that the highest gradient of the magnetic field (i.e., ∇H) occurs between the opposite poles (N-S) of the two adjacent magnets. Correspondingly, the applied field's gradient leads to the immense value of the exerted Kelvin body force to the ferrofluid. According to this figure, the exerted force and the other exerted force in the opposite direction can fluctuate the ferrofluid flow. Also, Based on the poles' positions of the magnets, all the appeared oscillations in the ferrofluid flow can form a continuous oscillation passing through the helical tube. This behavior can support the centrifugal force by intensifying the turbulence behavior of the fluid flow and decreasing the thickness of the sub-layer of the fluid near the hot wall.

It should be mentioned that the influence of the magnetic field on the thermal conductivity enhancement is highly dependent on the field direction [**29**]. This enhancement is due to the formation of chain-like aggregations. However, it seems that the chain's formation cannot be an effective parameter on the heat transfer enhancement in a non-uniform magnetic field [**29**]. Also, so long as the magnetic particles move by the fluid flow, the effect of forming the chain-like bridges may be less pronounced in the heat transfer enhancement [**5**].

For the more compelling case (φ=1.0% and $\dot{m}$=0.00415 kg/s), aforementioned in Section 3.3.1, **Fig. 9 (b)** shows the change in the temperature difference ($\Delta T_{oi} = T_o - T_i$) for different

remanent magnetizations compared to water. As shown from this figure, the collector's outlet temperature for the ferrofluid is higher than that of water. The higher the magnetic field strength, the more increased the collector's outlet temperature.

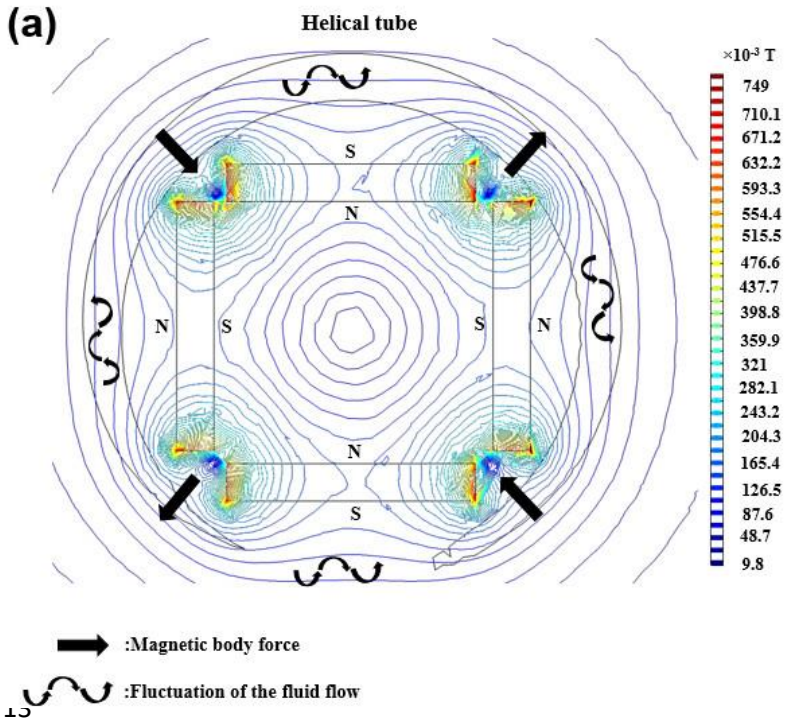

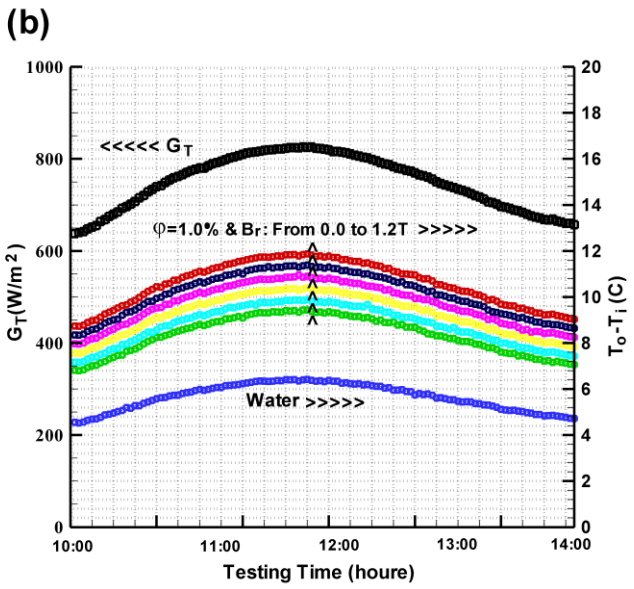

Fig. 9 (a) A virtual schematic of the affecting forces of the magnetic field (for B_r= 1.0 T) on the ferrofluid, and (b) effect of the different remanent magnetizations on the enhancement of the collector's outlet temperature for the case study with φ=1.0% and $\dot{m}$=0.00415 kg/s.

According to Eq. (11b), when the volume fraction has increased, the magnetization of the ferrofluid is increased, and correspondingly, Kelvin's body force (Eq. (11a)) is augmented. With increasing volume fraction, Kelvin's body force is more dominated over the viscous force [**5**]. Therefore, the higher the volume fraction, the more intensified the magnetic field effect on the collector efficiency enhancement. For the fluid flow rate of 0.00415 kg/s, **Fig. 10** shows a comparison among the three ferrofluid cases (i.e., φ= 0.2, 0.5, and 1.0%) and water when various remanent magnetizations (B_r= 0-1.2 T) are applied at the effective fluid flow rate (i.e., $\dot{m}$= 0.00415 kg/s).

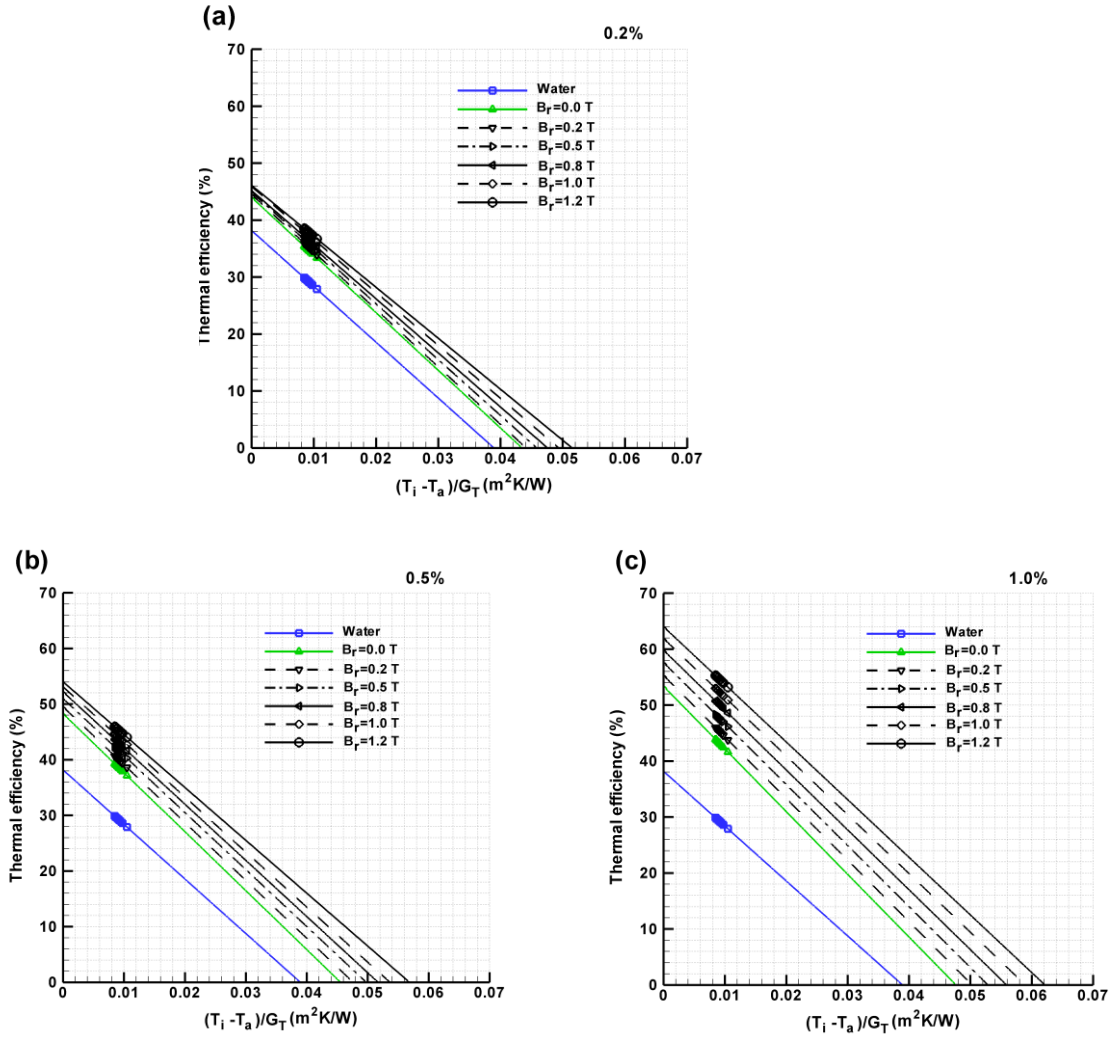

Fig. 10 The collector's thermal efficiency against $(T_i - T_a)/G_T$ at $\dot{m}$=0.00415 kg/s, for water, ferrofluid without a magnetic field, and ferrofluid under the influence of the various field's strengths of the magnets for the cases with (a) φ=0.2%, (b) φ=0.5%, and (c) φ=1.0%.

According to this figure, it is seen that the collector efficiency is increased with increasing volume fraction as well as the magnetic field. By moving from **Fig. 10 (a)** (i.e., φ= 0.2%) to

Fig. 10 (c) (i.e., φ= 1.0%), it is clear that the influence of the magnetic field on the collector efficiency enhancement is augmented with increasing nanoparticles volume fraction. Also, this efficiency augmentation appears to the whole range of solar radiation.

Furthermore, when various flow rates are studied, a constant competition between the magnetic force and the hydrodynamic forces is formed [**5**]. This behavior can be justified by considering the competition between the applied magnetic energy to the ferrofluid and the frictional energy between the suspended magnetic nanoparticles as the following non-dimensional ratio [**30**],

$$S = \frac{\text{magnetic energy}}{\text{frictional energy}} = \mathcal{M}Bd_p/(\lambda u) \quad (12)$$

where $\mathcal{M}$ is the nanoparticles' magnetization, B is the magnetic flux density, d_p is the nanoparticles' diameter, λ is the ferrofluid's viscosity, and u is the velocity.

At low values of the flow rate, the magnetic field has more opportunity to affect the magnetic nanoparticles and push (or pull) the ferrofluid toward the tube wall due to its body force. With the fluid flow augmentation, hydrodynamic forces dominate over the magnetic force, and the fluid flow carries away a large number of the magnetic nanoparticles. To put it another way, the formation of the magnetic moments is hindered by the hydrodynamic forces.

For the volume fraction of 1.0%, **Fig. 11** shows a comparison among the ferrofluid and water under various flow rates ($\dot{m}$= 0.00415-0.033 kg/s) when different remanent magnetizations (B_r= 0-1.2T) are applied at the effective volume fraction (i.e., $\dot{\varphi}$= 1.0%). According to this figure, by moving from **Fig. 11 (a)** to **Fig. 11 (d)**, it is clear that the suitable influence of the magnetic field on the collector efficiency augmentation of the collector is decreased with increasing fluid flow rate. So that, for the case with $\dot{m}$= 0.033 kg/s, with the magnetic field augmentation, the maximum collector efficiency ($F_R(\tau\alpha)$) is almost insignificant (the maximum increase has been 2.1%) except for a slight reduction (=5.5%) in the collector heat loss ($F_R U_L$) compared to the case without a magnetic field.

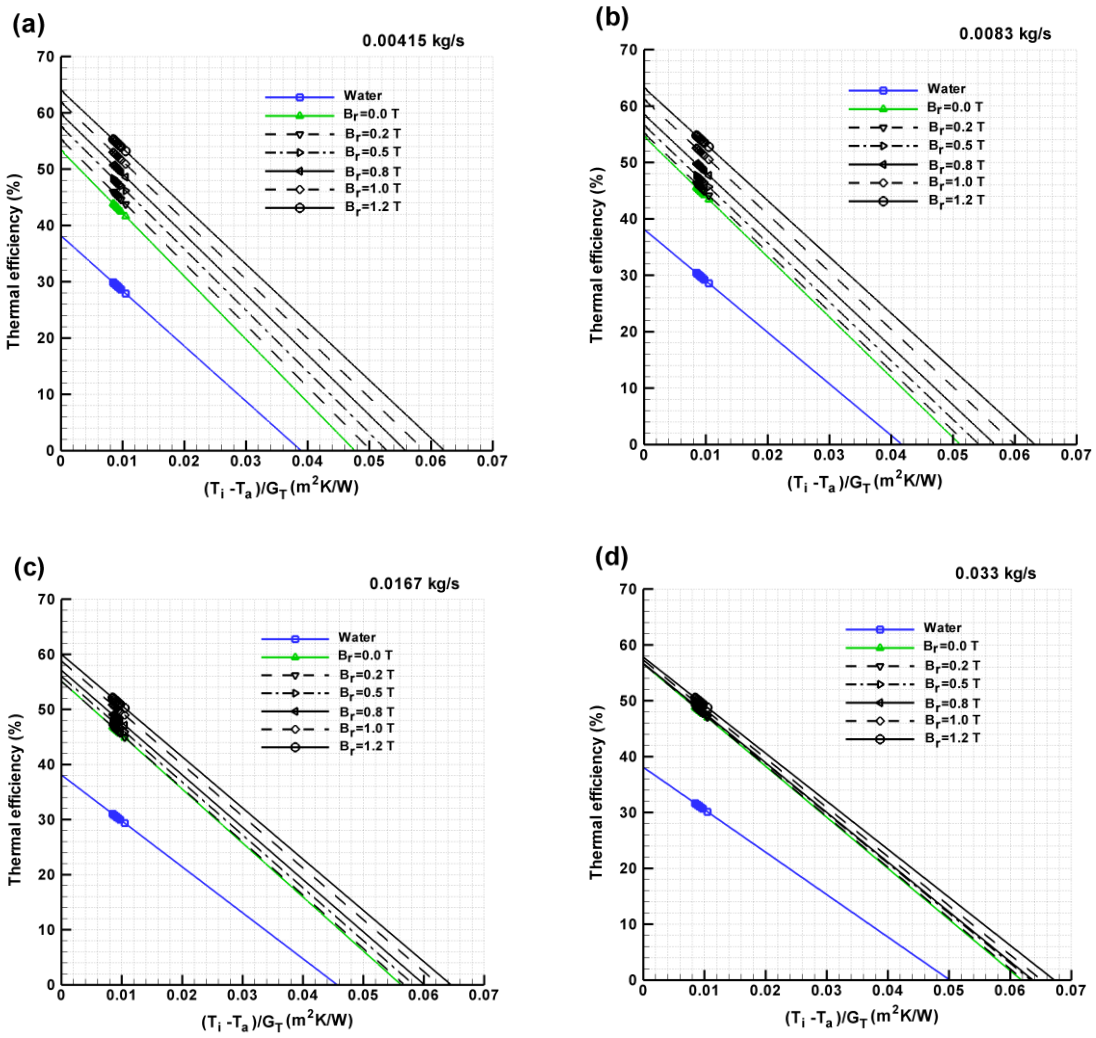

Fig. 11 The collector's thermal efficiency against $(T_i - T_a)/G_T$ at φ=1.0%, for water, ferrofluid without a magnetic field, and ferrofluid under the influence of the various strengths of the magnets for the cases with (a) $\dot{m}$=0.00415 kg/s, (b) $\dot{m}$=0.0083 kg/s, (c) $\dot{m}$=0.0167 kg/s, and (d) $\dot{m}$=0.033 kg/s.

Conclusions

The present experimental study investigated the advantage of using Mn–Zn Fe_2O_4/water ferrofluid subjected to the effect of the produced non-uniform magnetic field by a set of permanent magnets on the thermal efficiency of a cylindrical collector with a receiver in the shape of a helical pipe. Based on ASHRAE Standard, the investigation of the solar collector's efficiency was performed for various parameters, like nanoparticles volume fraction (0.0–1.0%), mass flow rate of the fluid (0.00415-0.033 kg/s), and remanent magnetization (B_r = 0.0–1.2 T).

According to the results, the overall thermal efficiency of the collector was increased with the volume fraction augmentation. For instance, without applying a magnetic field, the maximum collector efficiency enhancement compared with water has been 48.54% obtained for the case study with the volume fraction of 1.0% and the mass flow rate of 0.033 kg/s. Also, when the magnetic field was applied, the beneficial effect of the magnetic field due to the applied Kelvin body force predominated at lower flow rate values and higher volume fractions. For the case study with 0.00415 kg/s fluid flow rate and the volume fraction of 1.0%, by applying the magnets with B_r = 1.2T, the maximum thermal efficiency of the collector was increased by 67.67% compared with water.

The preparation process of the ferrofluid is almost similar to those of other nanofluids, and a well-stabilized ferrofluid can maintain its stability under the influence of the magnetic field. Finally, it can be generally concluded that the application of the ferrofluid subjected to the effect of the non-uniform magnetic field in the solar collector has an adequate ability to compete with other nanofluids. It should be noted that the permanent magnets have the advantage of long-lasting, and they are compatible with the collector's framing.

References

[**1**] R. Xin, M. Ebadian, The effects of Prandtl numbers on local and average convective heat transfer characteristics in helical pipes, J Heat Transf. 119 (1997) 467–473.

[**2**] K. Goudarzi, E. Shojaeizadeh, F. Nejati, An experimental investigation on the simultaneous effect of CuO-H_2O nanofluid and receiver helical pipe on the thermal efficiency of a cylindrical solar collector, APPL THERM ENG. 73 (2014) 1234-1241.

[**3**] K. Goudarzi, F. Nejati, E. Shojaeizadeh, S.K. Asadi Yousef-abad, Experimental study on the effect of pH variation of nanofluids on the thermal efficiency of a solar collector with helical tube, EXP THERM FLUID SCI. 60 (2015) 20–27.

[**4**] A.R. Noghrehabadi, E. Hajidavalloo, M. Moravej, An experimental investigation on the performance of a symmetric conical solar collector using SiO_2/water nanofluid, Trans. Phenom. Nano Micro Scales. 5(1) (2017) 23-29.

[**5**] M. H. Buschmann, Critical review of heat transfer experiments in ferrohydrodynamic pipe flow utilising ferronanofluids, INT J THERM SCI. https://doi.org/10.1016/j.ijthermalsci.2020.106426.

[**6**] N. Gan Jia Gui, C. Stanley, N.-T. Nguyen, G. Rosengarten, Ferrofluids for heat transfer enhancement under an external magnetic field, Int. J. Heat Mass Tran. 123 (2018) 110–121.

[**7**] Z. Liu, Y. Yan, R. Fu, M. Alsaady, Enhancement of solar energy collection with magnetic nanofluids, Therm. Sci. Eng. Prog. 8 (2018) 130–135.

[**8**] R. E. Rosensweig, Ferrohydrodynamics, DOVER PUBLICATIONS, INC. Mineola, New York, 1985, eISBN-13: 978-0-486-78300-0.

[**9**] G. Xu, Sh. Zhao, X. Zhang, X. Zhou, Experimental thermal evaluation of a novel solar collector using magnetic nano-particles, Energy Convers. Manage. 130 (2016) 252–259.

[**10**] M. Ameri, M. Syed Eshaghi, Exergy and thermal assessment of a Novel system utilizing flat plate collector with the application of nanofluid in porous media at a constant magnetic field, Therm. Sci. Eng. Prog. 8 (2018) 223–235.

[**11**] S. Sami, Impact of magnetic field on the enhancement of performance of thermal solar collectors using nanofluids, Int. J. Ambient Energy (2018), https://doi.org/10. 1080/01430750.2018.1437561.

[**12**] B.V. Balakin, O.V. Zhdaneev, A. Kosinska, Kirill V. Kutsenko, Direct absorption solar collector with magnetic nanofluid: CFD model and parametric analysis, Renew. Energy 136 (2019) 23-32

[**13**] A. Khosravi, M. Malekan, M.E.H. Assad, Numerical analysis of magnetic field effects on the heat transfer enhancement in ferrofluids for a parabolic trough solar collector, Renew. Energy 134 (2019) 54–63.

[**14**] M. Malekan, A. Khosravi, S. Syri, Heat Transfer Modeling of a Parabolic Trough Solar Collector with Working Fluid of Fe_3O_4 and CuO/Therminol 66 Nanofluids under Magnetic Field, Appl. Therm. Eng., DOI: https://doi.org/10.1016/j.applthermaleng.2019.114435.

[**15**] E. Shojaeizadeh, F. Veysi, K. Goudarzi, Heat transfer and thermal efficiency of a lab-fabricated ferrofluid-based single-ended tube solar collector under the effect of magnetic field: An experimental study, Appl. Therm. Eng. 164 (2020) 114510.

[**16**] M. Bezaatpour, H. Rostamzadeh, J. Bezaatpour, Hybridization of rotary absorber tube and magnetic field inducer with nanofluid for performance enhancement of parabolic trough solar collector, Journal of Cleaner Production, https://doi.org/10.1016/j.jclepro.2020.124565.

[**17**] M. Bahiraei, M. Hangi, Flow and heat transfer characteristics of magnetic nanofluids: A review, J Magn Magn Mater., http://dx.doi.org/10.1016/j. jmmm.2014.08.004i.

[**18**] Goldman, A.: Modern Ferrite Technology. Springer, New York (2006).

[**19**] ASHRAE Standard 86-93, Methods of Testing to Determine the Thermal Performance of Solar Collectors, Atlanta, GA, USA, 1986.

[**20**] S. Q. Zhou, R. Ni, Measurement of the specific heat capacity of water-based Al_2O_3 nanofluid, Appl. Phys. Lett. 92 (093123) (2008) 1-3.

[**21**] R. J. Moffat, Describing the uncertainties in experimental results, Exp. Therm. Fluid Sci. 1 (1988) 3–17.

[**22**] R.L. Manlapaz, S.W. Churchill, Fully developed laminar convection from a helical coil, Chem. Eng. Commun. 97 (1981) 185.

[**23**] M. Saedi, H. Aminfar, M. Mohammadpourfard, R. Maroofiazar, Simulation of ferrofluid flow boiling in helical tubes using two-fluid model, Heat and Mass Transfer (2019) 55:133–148.

[**24**] M. Sheikholeslami, D.D. Ganji, External Magnetic Field Effects on Hydrothermal Treatment of Nanofluid, William Andrew, Elsevier, 2016, pp. 1–354 (Print Book, ISBN: 9780323431385).

[**25**] S. Ahangar Zonouzi, R. Khodabandeh, H. Safarzadeh, H. Aminfar, Y. Trushkina, M. Mohammadpourfard, M. Ghanbarpour, G. Salazar Alvarez, Experimental investigation of the flow and heat transfer of magnetic nanofluid in a vertical tube in the presence of magnetic quadrupole field, EXP THERM FLUID SCI. 91 (2018) 155–165.

[**26**] M. Goharkhah, A. Salariana, M. Ashjaee, M. Shahabadi, Convective heat transfer characteristics of magnetite nanofluid under the influence of constant and alternating magnetic feld, Powder Technol. 274 (2015) 258–267.

[**27**] A. Abadeh, M. Mohammadi, Mohammad Passandideh-Fard, Experimental investigation on heat transfer enhancement for a ferrofluid in a helically coiled pipe under constant magnetic field, J THERM ANAL CALORIM. https://doi.org/10.1007/s10973-018-7478-2.

[**28**] M. Mohammadpourfard, H. Aminfar, M. Karimi, Numerical investigation of non-uniform transverse magnetic field effects on the swirling flow boiling of magnetic nanofluid in annuli, Int Commun Heat Mass Tranfer 75 (2016) 240–252.

[**29**] K. Parekh, Thermo-magnetic properties of ternary polydispersed $Mn_{0.5}Zn_{0.5}Fe_2O_4$ ferrite magnetic fluid, Solid State Communications 187 (2014) 33–37.

[**30**] M. Hejazian, N.-T. Nguyen, Magnetofluidic concentration and separation of non-magnetic particles using two magnet arrays, BIOMICROFLUIDICS 10 (044103) (2016) 1-11.

Figure Caption

Fig. 1 (a) XRD of Mn–Zn Ferrite nanomaterial, (b) Hysteresis loop of the prepared nanoparticles, and (c) Zeta potential at various times

Fig. 2 (a) Schematic of the experimental setup: (1) helical Cu tube, (2) arrangement of the permanent magnets (quadrupole), (3) cylindrical glass, (4) working fluid supply, (5) pump, (6) drain, (7) line valve, (8) flowmeter, (9) tank, (10) heat exchanger, (11) cold water inlet, (12) hot water inlet, (13) collector inlet thermocouple, (14) collector outlet thermocouple, (15) air temperature thermocouple, and (16) thermometer; (b) a photograph of the experimental setup; and (c) distribution of the vectors of the magnetic field produced by the magnets at an axial cross-section.

Fig. 3 A testing day for the case with water at 0.00415 kg/s mass flow rate of the fluid.

Fig. 4 The collector's thermal efficiency against $(T_i - T_a)/G_T$ for water at different fluid flow rates.

Fig. 5 $F_R(\tau\alpha)$ and $F_R U_L$ variations for the ferrofluid (with (a) 0.2%, (b) 0.5%, and (c) 1.0%) at various flow rates compared with water.

Fig. 6 $F_R(\tau\alpha)$ values for the ferrofluid (with (a) 0.2%, (b) 0.5%, and (c) 1.0%) at various flow rates under the effect of various remanent magnetizations.

Fig. 7 Subtraction between $F_R(\tau\alpha)$ and $F_R U_L$ variations for the ferrofluid (with (a) 0.2%, (b) 0.5%, and (c) 1.0%) at various flow rates under the effect of various remanent magnetizations compared with water.

Fig. 8 Distributed magnetic flux density using the set of magnets with B_r= 1.0 T.

Fig. 9 (a) A virtual schematic of the affecting forces of the magnetic field (for B_r= 1.0 T) on the ferrofluid, and (b) effect of the different remanent magnetizations on the enhancement of the collector's outlet temperature for the case study with φ=1.0% and $\dot{m}$=0.00415 kg/s.

Fig. 10 The collector's thermal efficiency against $(T_i - T_a)/G_T$ at $\dot{m}$=0.00415 kg/s, for water, ferrofluid without a magnetic field, and ferrofluid under the influence of the various field's strengths of the magnets for the cases with (a) φ=0.2%, (b) φ=0.5%, and (c) φ=1.0%.

Fig. 11 The collector's thermal efficiency against $(T_i - T_a)/G_T$ at φ=1.0%, for water, ferrofluid without a magnetic field, and ferrofluid under the influence of the various strengths of the magnets for the cases with (a) $\dot{m}$=0.00415 kg/s, (b) $\dot{m}$=0.0083 kg/s, (c) $\dot{m}$=0.0167 kg/s, and (d) $\dot{m}$=0.033 kg/s.

Table Caption

Table 1 General specifications of the setup.

Table 2 Thermal efficiency parameters of the collector for water with various fluid flow rates.

Table 3 $F_R(\tau\alpha)$ and $F_R U_L$ values for the ferrofluid at different volume fractions and various fluid flow rates.

Table 4 $F_R(\tau\alpha)$ and $F_R U_L$ values at various volume fractions, fluid flow rates, and remanent magnetizations.

Table 5 A comparison between $F_R(\tau\alpha)$ increase compared with water in the present study and those obtained by Goudarzi et al. [**2-3**].